

## Topological Phase Transitions Driven by Magnetic Phase Transitions in $\text{Fe}_x\text{Bi}_2\text{Te}_3$ ( $0 \leq x \leq 0.1$ ) Single Crystals

Heon-Jung Kim,<sup>1,\*</sup> Ki-Seok Kim,<sup>2</sup> J.-F. Wang,<sup>3</sup> V. A. Kulbachinskii,<sup>4</sup> K. Ogawa,<sup>5</sup> M. Sasaki,<sup>6</sup> A. Ohnishi,<sup>6</sup> M. Kitaura,<sup>6</sup> Y.-Y. Wu,<sup>3</sup> L. Li,<sup>3</sup> I. Yamamoto,<sup>5</sup> J. Azuma,<sup>5</sup> M. Kamada,<sup>5</sup> and V. Dobrosavljević<sup>7</sup>

<sup>1</sup>*Department of Physics, College of Natural Science, Daegu University, Gyeongsbuk 712-714, Republic of Korea*

<sup>2</sup>*Department of Physics, Pohang University of Science and Technology, Pohang, Gyeongsbuk 790-784, Republic of Korea*

<sup>3</sup>*Wuhan National High Magnetic Field Center, Huazhong University of Science and Technology, Wuhan 430074, China*

<sup>4</sup>*Physics Department, Moscow State University, Moscow 119899, Russia*

<sup>5</sup>*Synchrotron Light Application Center, Saga University, Honjo, Saga 840-8502, Japan*

<sup>6</sup>*Department of Physics, Faculty of Science, Yamagata University, Kojirakawa, Yamagata 990-8560, Japan*

<sup>7</sup>*Department of Physics and National High Magnetic Field Laboratory, Florida State University, Tallahassee, Florida 32306, USA*

(Received 6 August 2012; revised manuscript received 4 December 2012; published 25 March 2013)

We propose a phase diagram for  $\text{Fe}_x\text{Bi}_2\text{Te}_3$  ( $0 \leq x \leq 0.1$ ) single crystals, which belong to a class of magnetically bulk-doped topological insulators. The evolution of magnetic correlations from ferromagnetic to antiferromagnetic gives rise to topological phase transitions, where the paramagnetic topological insulator of  $\text{Bi}_2\text{Te}_3$  turns into a band insulator with ferromagnetic-cluster glassy behavior around  $x \sim 0.025$ , and it further evolves to a topological insulator with valence-bond glassy behavior, which spans over the region from  $x \sim 0.03$  up to  $x \sim 0.1$ . This phase diagram is verified by measuring magnetization, magnetotransport, and angle-resolved photoemission spectra with theoretical discussions.

DOI: [10.1103/PhysRevLett.110.136601](https://doi.org/10.1103/PhysRevLett.110.136601)

PACS numbers: 72.90.+y, 71.27.+a, 75.20.Hr, 75.47.-m

The characteristic features of topological insulators originate from the existence of topologically protected gapless surface states [1–4], which gives rise to anomalous transport phenomena [5]. In particular, an anomalous Hall effect of the topological origin and extremely large magnetoresistance (MR) have been observed and attributed to surface Dirac electrons [6]. For scientific understanding and practical applications, such anomalous transport needs to be controlled, for example, by creating magnetic correlations in topological insulators. In fact, several surface- and bulk-doping studies [7–11] reported that surface-doped magnetic impurities are aligned ferromagnetically to cause an excitation gap for surface Dirac electrons [7,8]. However, the gap opening was not always observed [9–11], which suggests that Ruderman-Kittel-Kasuya-Yosida (RKKY) interactions by surface Dirac electrons may be more complicated than expected. Indeed, such RKKY interactions consist of Heisenberg-like, Ising-like, and Dzyaloshinskii-Moriya (DM)-like terms, and are expected to cause frustration for spin dynamics [12–14]. As a result, various spin orders are expected to occur due to interplay between the randomness and spin-orbit interaction provided the chemical potential lies away from the Dirac point of the surface band. This aspect motivated us to dope magnetic ions into the bulk of a topological insulator, controlling anomalous transport phenomena.

In this Letter, we examine the effects of various spin orders on topological properties in  $\text{Fe}_x\text{Bi}_2\text{Te}_3$  ( $0 \leq x \leq 0.1$ ) single crystals by measuring the MR, Hall resistance, magnetization, and angle-resolved photoemission spectroscopy (ARPES). Transport properties change

drastically, following the evolution of magnetic correlations in the bulk. The Curie-Weiss temperature  $\theta$  initially increases with  $x$ , reaching a maximum at  $x = 0.025$ . This indicates enhancement of ferromagnetic correlations around  $x = 0.025$ . Such predominant ferromagnetic correlations turn out to reflect more complicated spin dynamics associated with random positions of magnetic ions. Ferromagnetic-cluster glassy behavior is observed around this  $x$  value along with drastic changes in the MR and Hall effect. The characteristic features of topological-insulator samples, such as large MR and anomalous Hall effect, are no longer observed in the  $\text{Fe}_{0.025}\text{Bi}_2\text{Te}_3$  sample, which suggests that a gap opens at the Dirac point of the surface band. Indeed, we observe the gap opening from our ARPES measurement. Interestingly,  $\text{Fe}_x\text{Bi}_2\text{Te}_3$  samples with  $x = 0.05$  and  $0.1$  exhibit essentially the same transport behavior as undoped  $\text{Bi}_2\text{Te}_3$  without any sign of ferromagnetism. Furthermore, ARPES fails to detect any gap opening at the Dirac point in the  $\text{Fe}_{0.1}\text{Bi}_2\text{Te}_3$  sample, confirming the recovery of the topologically nontrivial nature. This puzzling observation of the reentrant behavior is resolved, considering that the Weiss temperature  $\theta$  becomes negative above  $x = 0.025$ , where antiferromagnetic correlations become more dominant than ferromagnetic interactions, giving rise to valence-bond glassy behavior. The entire result is summarized in the phase diagram of Fig. 1.

The powder x-ray diffraction (XRD) data, measured by using crushed  $\text{Fe}_x\text{Bi}_2\text{Te}_3$  crystals with  $x = 0.0, 0.025, 0.05, 0.075,$  and  $0.1$  are shown in Fig. 2(a). The experimental details are explained in the Supplemental Material

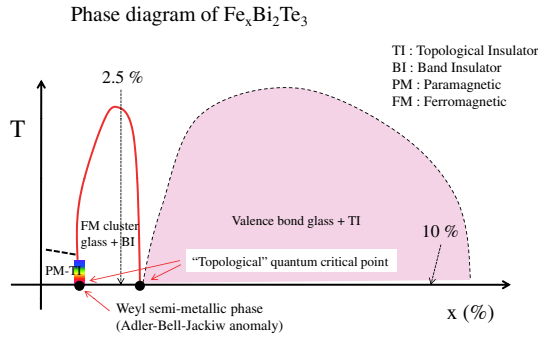


FIG. 1 (color online). Phase diagram and topological phase transitions of  $\text{Fe}_x\text{Bi}_2\text{Te}_3$ .

[15]. The XRD neither showed any significant change of the  $\text{Bi}_2\text{Te}_3$  structure nor exhibited the appearance of superstructures. Figure 2(b) shows the  $M(T)$  curves of the  $\text{Fe}_x\text{Bi}_2\text{Te}_3$  single crystals under magnetic fields perpendicular to the cleaved (111) plane. In addition, the inset in Fig. 2(b) displays  $1/M(T)$  for the samples with  $x = 0.0125, 0.05,$  and  $0.1$ . Clearly, these curves are linear in the high temperature region, which indicates that they follow the Curie-Weiss law. At lower temperatures, the  $M(T)$  curves deviate from this linearity, the temperature of which depends on  $x$  as spin correlations develop. In particular, the

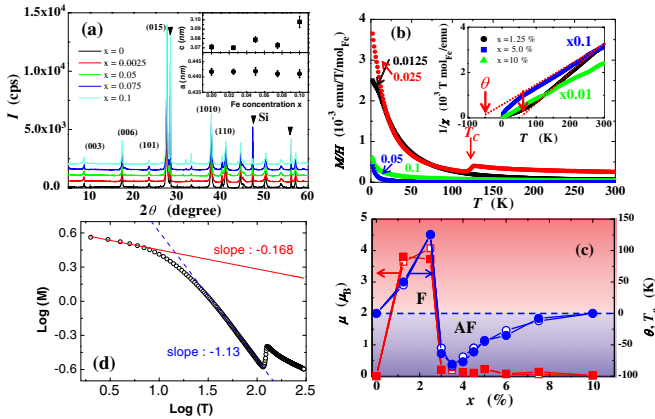


FIG. 2 (color online). (a) Powder x-ray diffraction data of  $\text{Fe}_x\text{Bi}_2\text{Te}_3$  samples with  $x = 0.0, 0.025, 0.05, 0.075,$  and  $0.1$  from the bottom of the figure. The upper and lower insets show the  $c$  and  $a$  parameters, respectively, as a function of Fe concentrations. The  $c$  parameter slightly increases with increasing  $x$  while the  $a$  parameter is almost unchanged. (b) Temperature dependence of  $M/H$  for  $\text{Fe}_x\text{Bi}_2\text{Te}_3$  with  $x = 0.0125, 0.025, 0.05,$  and  $0.1$  for the magnetic fields perpendicular (111) plane. The inset shows  $1/M$  curves with Curie-Weiss fitting. (c) The Weiss temperature  $\theta$  or Curie temperature  $T_c$  and the magnetic moment  $\mu$  determined from the Curie-Weiss fitting as a function of  $x$ . The open (closed) circles are the Weiss temperatures for the magnetic field parallel (perpendicular) to the (111) plane. The open (closed) squares are the magnetic moments determined for the magnetic field parallel (perpendicular) to the (111) plane. (d) The log-log plot of the  $M(T)$  curve for  $x = 0.025$ , along with the linear fits at high and low temperatures.

sample with  $x = 0.025$  shows a very clear deviation or a hump at approximately  $T = 120$  K in the original  $M(T)$  curve. To clarify the nature of this behavior, the  $M(T)$  curves were fitted to the Curie-Weiss formula,  $M(T)/H = C/(T + \theta)$  with a constant  $C = N\mu_{\text{eff}}^2/(3k_B)$ , where  $N$  is the number of impurities,  $\mu_{\text{eff}}$  is the effective magnetic moment, and  $k_B$  is the Boltzmann constant. The inset of Fig. 2(b) shows our results of fitting, plotted as dotted (red) lines. The Curie-Weiss temperatures  $\theta$  of the samples with  $x = 0.0125$  and  $0.05$  are positive and negative, respectively, while it becomes almost zero in the sample with  $x = 0.1$ . This suggests that average magnetic interactions change around  $x = 0.025$  from ferromagnetic to antiferromagnetic correlations.

To understand the change of magnetic correlations in more detail, we present the Weiss temperature and effective magnetic moment in Fig. 2(c), determined from the Curie-Weiss fitting to the  $M(T)$  curves as a function of  $x$ . For  $x \leq 0.025$ , the Weiss temperature increases with  $x$ , reaching a maximum at  $x = 0.025$ . The maximum Weiss temperature suggests that ferromagnetic correlations are predominant around  $x = 0.025$ . On the other hand, such average magnetic correlations change drastically from ferromagnetic to antiferromagnetic interactions around  $x = 0.03$ . The negative  $\theta$  for  $x > 0.025$  is attributed to the enhancement of antiferromagnetic correlations. The average magnetic moment also shows a sudden decrease just above  $x \sim 0.025$ , again indicating that predominant magnetic correlations change from ferromagnetic to antiferromagnetic across this particular  $x$  value.

We would like to emphasize that such average magnetic correlations, reflected in Curie-Weiss temperatures and magnetic moments, hide more complicated spin dynamics. Although the susceptibility curve for  $x = 0.0125$  increases monotonically, the fact that it saturates to a finite value at  $T = 0$  implies that not only ferromagnetic correlations but also antiferromagnetic interactions play their certain roles in this random system of magnetic impurities, giving rise to glassy behavior. The cusp around 130 K seems to indicate that random magnetic interactions are at work. In addition, the continuous increase with a power-law behavior but the change of its slope around 15 K and the saturation of such divergent behaviors at the lowest temperature imply that magnetic correlations evolve from quantum Griffiths behaviors to ferromagnetic-cluster glassy structures. If a magnetically doped system shows about 70% ferromagnetic interactions and 30% antiferromagnetic correlations due to randomly distributed positions of magnetic ions, it is natural to expect that ferromagnetic clusters are formed and their random spin correlations can result in glassy behavior through intermediate complex spin dynamics.

Actually, quantum Griffiths behaviors can be verified by the measurement of the exponent in the temperature

dependence of magnetization,  $M \sim T^{-\alpha}$ . A broad distribution of sizes of such clusters and their effective interactions to other clusters has been claimed to cause the exponent  $\alpha$  to be less than 1 [16]. Indeed, we observe such spin dynamics as shown in Fig. 2(d). Just below the cusp, the value of  $\alpha$  is around 1. On the other hand, it becomes much reduced to 0.163 from approximately 15 K, indicating the signature of the quantum Griffiths phase [17]. As temperature decreases further, these ferromagnetic clusters become frozen. As a result, the divergent behavior weakens, the spin susceptibility being saturated to a finite value. As the concentration of magnetic impurities increases, predominant magnetic correlations evolve from ferromagnetic to antiferromagnetic, verified from the Curie-Weiss plot at  $x = 0.05$  and 0.1, discussed before. Considering that the spin susceptibility increases but saturates at low temperatures, we speculate that the ground state is a sort of “spin liquid,” which may correspond to valence-bond glassy behavior.

The observed change in the spin dynamics profoundly affects the magnetotransport properties of  $\text{Fe}_x\text{Bi}_2\text{Te}_3$  single crystals. Figure 3 shows the MR ( $= \Delta\rho/\rho_0$ ) and Hall resistance of  $\text{Bi}_2\text{Te}_3$ ,  $\text{Fe}_{0.025}\text{Bi}_2\text{Te}_3$ , and  $\text{Fe}_{0.1}\text{Bi}_2\text{Te}_3$  single crystals at 4.2 K. The MR and Hall resistance of  $\text{Bi}_2\text{Te}_3$  are typical of the as-grown  $\text{Bi}_2\text{Te}_3$  single crystals as reported previously [6]. The observed MR is  $\sim 100\%$  at 4 T and the Hall resistance is nonlinear due to anomalous Hall effects from Berry phase, side jump, and skew scattering contributions [6]. Because the  $\text{Bi}_2\text{Te}_3$  in this study is an as-grown sample, the bulk conduction channel still exists with a  $p$ -type charge carrier. As shown in Fig. 3, there is no qualitative difference between  $\text{Bi}_2\text{Te}_3$  and  $\text{Fe}_{0.1}\text{Bi}_2\text{Te}_3$ . It should be noted that both the MR and Hall resistance of the samples with  $x = 0, 0.0125, 0.05, 0.075$ , and 0.1

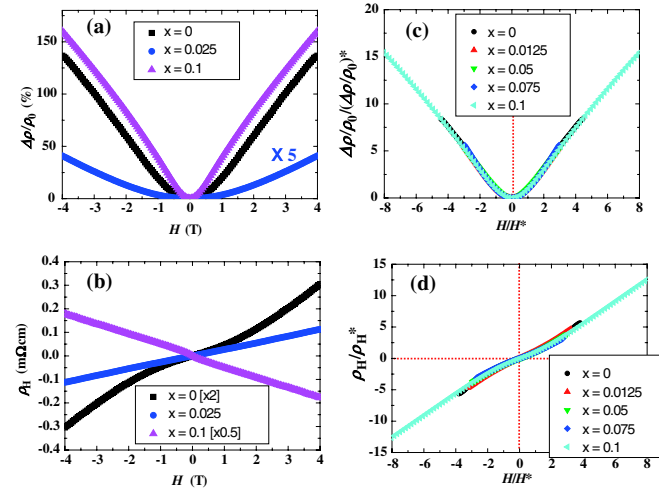


FIG. 3 (color online). (a) The MR and (b) Hall resistance as a function of  $H$  for  $p$ -doped  $\text{Bi}_2\text{Te}_3$  (square),  $\text{Fe}_{0.025}\text{Bi}_2\text{Te}_3$  (circle), and  $\text{Fe}_{0.1}\text{Bi}_2\text{Te}_3$  (triangle) single crystals. The scaling behaviors of (c) MR and (d) Hall resistance for  $\text{Fe}_x\text{Bi}_2\text{Te}_3$  with  $x = 0, 0.0125, 0.05, 0.075$ , and 0.1.

scaled by the proper  $\text{MR}^*$ 's and  $H^*$ 's as shown in Figs. 3(c) and 3(d), respectively, in which  $H^*$  is a characteristic field characterizing surface conduction due to Dirac fermions and  $\text{MR}^*$  is the MR at  $H = H^*$ . Therefore, the features related to the surface conduction, such as large MR and anomalous Hall effect, are still observable in  $\text{Fe}_{0.1}\text{Bi}_2\text{Te}_3$ , suggesting the survival of surface conduction.

In contrast, the MR and Hall resistance of  $\text{Fe}_{0.025}\text{Bi}_2\text{Te}_3$  are quite different and completely conventional in that the MR and Hall resistance are quadratic and linear with  $H$  up to 4 T, respectively. The magnitude of MR, which is approximately 8% at 4 T, is reduced drastically compared to  $\text{Bi}_2\text{Te}_3$  and  $\text{Fe}_{0.1}\text{Bi}_2\text{Te}_3$ . This sample simply follows the Boltzmann transport theory. Therefore, the surface conduction by Dirac fermions appears to be suppressed completely. In addition, the hole mobility  $\mu$  and the hole number  $p$  estimated from the quadratic MR and linear Hall resistance are  $0.14 \text{ m}^2/\text{Vs}$  and  $1.8 \times 10^{19} \text{ cm}^{-3}$ , respectively, which are in a range of conventional doped semiconductors. This also supports the bulk electrical

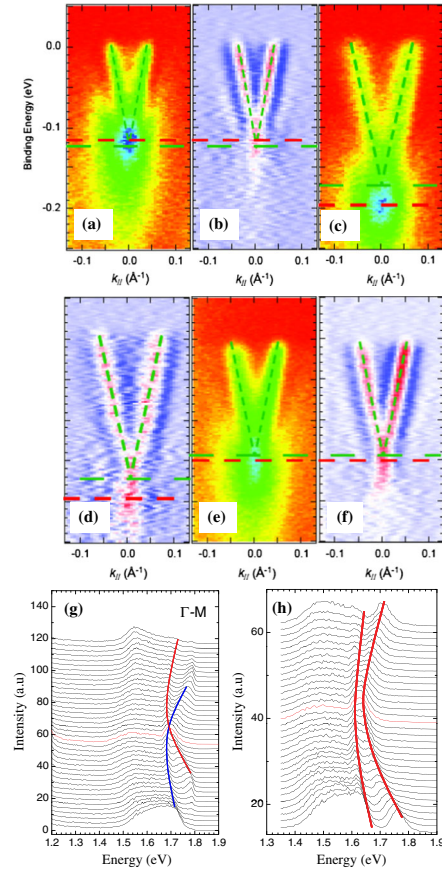


FIG. 4 (color online). The photoemission intensity plots of (a)  $\text{Bi}_2\text{Te}_3$ , (c)  $\text{Fe}_{0.025}\text{Bi}_2\text{Te}_3$ , and (e)  $\text{Fe}_{0.1}\text{Bi}_2\text{Te}_3$ , taken by using a synchrotron along the  $\Gamma$ - $M$  lines. The dashed lines are the fitting curves, determined from the momentum distribution curves. (b), (d), and (f) are their second derivatives. The energy distribution curves of (g)  $\text{Bi}_2\text{Te}_3$  and (h)  $\text{Fe}_{0.025}\text{Bi}_2\text{Te}_3$  along the  $\Gamma$ - $M$  lines, measured using the vacuum ultraviolet laser source.

conduction in this sample. Predominant ferromagnetic correlations and conventional behaviors of electrical transport properties observed at the  $x = 0.025$  samples are quite correlated.

The changes of the magnetic and transport properties are accompanied by the change of the surface electronic states. Figures 4(a)–4(f) are the photoemission intensities and their second derivatives of  $\text{Bi}_2\text{Te}_3$ ,  $\text{Fe}_{0.025}\text{Bi}_2\text{Te}_3$ , and  $\text{Fe}_{0.1}\text{Bi}_2\text{Te}_3$ , respectively, along the  $\Gamma$ - $M$  lines. The Fermi levels of these ARPES spectra were observed to change with time, which seems to be a feature of the  $\text{Bi}_2\text{Te}_3$  surface not related to the intrinsic band structure [18]. Because of this, the Fermi levels of the spectra are different. To resolve the dispersions of the surface Dirac bands clearly, the peak positions are determined from the momentum distribution curves by fitting. These peak positions at different energies give the dashed lines in Figs. 4(a)–4(f). In  $\text{Bi}_2\text{Te}_3$  and  $\text{Fe}_{0.1}\text{Bi}_2\text{Te}_3$ , the dispersions are linear near the Dirac point virtually with no gap, implying the existence of the surface Dirac states. On the other hand, in  $\text{Fe}_{0.025}\text{Bi}_2\text{Te}_3$ , the dispersion has a gap of 30–40 meV, suggesting a time-reversal-symmetry broken surface state. The gap opening at the Dirac point in  $\text{Fe}_{0.025}\text{Bi}_2\text{Te}_3$  was also observed in our laser-ARPES experiments. Figures 4(g) and 4(h) present the stacks of energy distribution curves of  $\text{Bi}_2\text{Te}_3$  and  $\text{Fe}_{0.025}\text{Bi}_2\text{Te}_3$ , respectively. The laser-ARPES experiment also demonstrates the linear dispersion near the Dirac point in  $\text{Bi}_2\text{Te}_3$ . In contrast, the surface bands in  $\text{Fe}_{0.025}\text{Bi}_2\text{Te}_3$  have a gap of 30–40 meV, consistent with the synchrotron-based ARPES results.

Our experiments reported one type of a magnetic phase transition from a ferromagnetic-cluster glassy state to a valence-bond glassy phase, where predominant magnetic correlations change from ferromagnetic to

antiferromagnetic and at least two topological phase transitions. The first occurs in the region where predominant ferromagnetic correlations exist while the second seems to appear at the magnetic phase transition.

The magnetic phase transition itself is not unexpected because RKKY interactions between doped magnetic impurities can change from ferromagnetic to antiferromagnetic, depending on their distances. Although a band-structure calculation is needed to understand the nature of the RKKY interactions more accurately, one can estimate the order of magnitude for the critical concentration of magnetic ions that corresponds to a change in the sign of the RKKY interaction. Because the RKKY interaction oscillates on the length scale of  $1/2k_F$ , a sign change occurs when the number of the magnetic impurities becomes comparable with  $L^3(2k_F)^3$ , where  $L$  is the lateral size of a sample. Taking the critical concentration of  $x_c \sim 0.025$  with simple algebra produces  $k_F \approx 10^7\text{--}10^8 \text{ cm}^{-1}$ , which corresponds to the Fermi energy  $E_F \sim 0.01\text{--}0.1 \text{ eV}$  with the effective mass of  $\text{Bi}_2\text{Te}_3$ . This is in agreement with conventional values estimated by ARPES and de Haas–van Alphen experiments [19].

Two kinds of topological phase transitions can be understood in the following way. The first topological phase transition in the region of  $x < 0.025$  is driven by ferromagnetic-cluster glassy behavior, where magnetic phase transitions are not accompanied. On the other hand, the second topological phase transition appears to be driven by the magnetic phase transition from a cluster glassy state to a valence-bond glassy phase, where predominant ferromagnetic interactions evolve into antiferromagnetic correlations. We suggest an effective free-energy functional as a phenomenological model for these topological phase transitions,

$$\begin{aligned} \mathcal{F}_{MF}[\Phi(I), b(I), \chi(I), \lambda(I); T] = & -T \int dIP[I] \ln \int D\psi_{\sigma\tau}(\mathbf{r}) Df_{\sigma}(\mathbf{r}) \exp \left[ - \int_0^{1/T} d\tau \int \frac{d^3\mathbf{k}}{(2\pi)^3} \psi_{\sigma\tau}^\dagger(\mathbf{k}) \{ (\partial_\tau - \mu) \mathbf{I}_{\sigma\sigma'} \otimes \mathbf{I}_{\tau\tau'} \right. \\ & + \mathbf{v}\mathbf{k} \cdot \boldsymbol{\sigma}_{\sigma\sigma'} \otimes \boldsymbol{\tau}_{\tau\tau'}^z + m(|\mathbf{k}|) \mathbf{I}_{\sigma\sigma'} \otimes \boldsymbol{\tau}_{\tau\tau'}^x \} \psi_{\sigma'\tau'}(\mathbf{k}) - \int_0^{1/T} d\tau \int d^3\mathbf{r} J \psi_{\sigma\tau}^\dagger(\mathbf{r}) \\ & \times (\boldsymbol{\sigma}_{\sigma\sigma'} \otimes \mathbf{I}_{\tau\tau'}) \psi_{\sigma'\tau'}(\mathbf{r}) \cdot \Phi - \int_0^{1/T} d\tau \int \frac{d^3\mathbf{k}}{(2\pi)^3} \{ f_{\sigma}^\dagger(\mathbf{k}) (\partial_\tau + \lambda + I\chi\epsilon_{\mathbf{k}}^f) f_{\sigma}(\mathbf{k}) \\ & + I f_{\sigma}^\dagger(\mathbf{k}) (\Phi \cdot \boldsymbol{\sigma})_{\sigma\sigma'} f_{\sigma'}(\mathbf{k}) - b(\psi_{\sigma\tau}^\dagger(\mathbf{k}) f_{\sigma}(\mathbf{k}) + f_{\sigma}^\dagger(\mathbf{k}) \psi_{\sigma\tau}(\mathbf{k})) \} \\ & \left. - \frac{L^3}{T} \left( \lambda + zI\chi^2 - I\Phi \cdot \Phi + \frac{b^2}{J} \right) \right], \end{aligned}$$

where topological insulators and doped magnetic ions are described by  $\psi_{\sigma\tau}$  and  $f_{\sigma}$  with spin  $\sigma$  and band  $\tau$ , respectively.  $\Phi$  is a ferromagnetic order parameter that controls the first topological phase transition, and  $\chi$  is a valence-bond singlet order parameter that drives the second topological phase transition when predominant magnetic correlations become antiferromagnetic.  $b$  is a hybridization parameter associated with the Kondo effect and  $\lambda$  is a

Lagrange multiplier field to impose the single occupancy constraint for impurity spins. An important point is that the distribution function  $P[I]$  of magnetic correlations can be determined by fitting our experimental data of the spin susceptibility. Then, one finds order parameters as a function of  $I$ , which determine the phase diagram of Fig. 1. See our Supplemental Material for more detailed discussions [15]. Solving self-consistent equations for

order parameters remains as the future direction of our research.

The present study may shed light on the previous controversial results about gap opening of the surface Dirac band. Recall that Ref. [8] reported the gap opening, while the later ARPES studies of Refs. [9,11] claimed the opposite with virtually no difference between magnetic and nonmagnetic ions. These null results are more consistent with the reported positions of the Fermi level far from the Dirac point, which favors ferromagnetism with in-plane moments, not causing the gap to open. In this respect, the bulk doping of magnetic ions is more effective than the surface doping for controlling the topological characters. Indeed, the gapped surface state was realized by magnetically bulk doping [7]. Our suggested phase diagram is quite general and can also explain other cases such as Fe-doped  $\text{Bi}_2\text{Se}_3$  [7] and  $\text{Bi}_{2-x}\text{Mn}_x\text{Te}_3$  [20], where the ferromagnetic “insulating” region is more expanded than the present case. The phase boundary and the area of each phase in Fig. 1 will be determined by the periodicity of the RKKY interaction, given by  $1/2k_F$ . We suspect that our doped samples are more metallic than those of the previous works. Therefore, in our case the Fermi momentum  $k_F$  is relatively larger and the ferromagnetic-interaction dominated region is smaller, allowing us to observe topological phase transitions.

In conclusion, our experiments verified magnetically controlled topological phase transitions by doping magnetic ions into topological insulators. The transport properties of both MR and Hall become normal at low concentrations ( $x \leq x_c$ ) around ferromagnetic-cluster glassy behavior. At high concentrations ( $x \geq x_c$ ), they turn abnormal, essentially identical to those of topological insulators, when antiferromagnetic correlations are predominant. A phase diagram of  $\text{Fe}_x\text{Bi}_2\text{Te}_3$  ( $0 \leq x \leq 0.1$ ) single crystals was proposed, based on the magnetization, transport measurements, ARPES, and theoretical discussions. The present study casts a new theoretical challenge, in particular, on how to characterize or define topological phase transitions in the presence of randomly distributed magnetic clusters. This conceptual framework generalizes the physics of dilute magnetic semiconductors [21], introducing topological aspects of electronic structures.

This research is supported by the Basic Science Research Program through the National Research Foundation of Korea (NRF) funded by the Ministry of Education, Science, and Technology (Grant No. 2012-0007294). K.-S. K. was supported by the National Research Foundation of Korea (NRF) and funded by the Korea government (MEST) (Grant No. 2012000550). V. D. was supported by NSF Grant No. DMR-1005751. M. S. expresses his thanks to Professor T. Iwata and Professor K. Tomita for valuable discussions and support.

\*Corresponding author.

hjkim76@daegu.ac.kr

- [1] C.L. Kane and E.J. Mele, *Phys. Rev. Lett.* **95**, 146802 (2005); **95**, 226801 (2005).
- [2] L. Fu, C.L. Kane, and E.J. Mele, *Phys. Rev. Lett.* **98**, 106803 (2007); L. Fu and C.L. Kane, *Phys. Rev. B* **76**, 045302 (2007).
- [3] J.E. Moore and L. Balents, *Phys. Rev. B* **75**, 121306 (2007).
- [4] R. Roy, *Phys. Rev. B* **79**, 195322 (2009); **79**, 195321 (2009).
- [5] Dong-Xia Qu, Y. S. Hor, Jun Xiong, R. J. Cava, and N. P. Ong, *Science* **329**, 821 (2010).
- [6] Heon-Jung Kim, Ki-Seok Kim, Mun Dae Kim, S.-J. Lee, J.-W. Han, A. Ohnishi, M. Kitaura, M. Sasaki, A. Kondo, and K. Kindo, *Phys. Rev. B* **84**, 125144 (2011).
- [7] Y.L. Chen, J.-H. Chu, J.G. Analytis, Z.K. Liu, K. Igarashi, H.-H. Kuo, X.L. Qi, S.K. Mo, R.G. Moore, D.H. Lu, M. Hashimoto, T. Sasagawa, S.C. Zhang, I.R. Fisher, Z. Hussain, and Z.X. Shen, *Science* **329**, 659 (2010).
- [8] L.A. Wray, S.-Y. Xu, Y. Xia, D. Hsieh, A.V. Fedorov, Y.S. Hor, R.J. Cava, A. Bansil, H. Lin, and M.Z. Hasan, *Nat. Phys.* **7**, 32 (2011).
- [9] T. Valla, Z.-H. Pan, D. Gardner, Y.S. Lee, and S. Chu, *Phys. Rev. Lett.* **108**, 117601 (2012).
- [10] Y.S. Hor, P. Roushan, H. Beidenkopf, J. Seo, D. Qu, J.G. Checkelsky, L.A. Wray, D. Hsieh, Y. Xia, S.-Y. Xu, D. Qian, M.Z. Hasan, N.P. Ong, A. Yazdani, and R.J. Cava, *Phys. Rev. B* **81**, 195203 (2010).
- [11] M.R. Scholz, J. Sánchez-Barriga, D. Marchenko, A. Varykhalov, A. Volykhov, L.V. Yashina, and O. Rader, *Phys. Rev. Lett.* **108**, 256810 (2012).
- [12] J.-J. Zhu, D.-X. Yao, S.-C. Zhang, and K. Chang, *Phys. Rev. Lett.* **106**, 097201 (2011).
- [13] D.A. Abanin and D.A. Pesin, *Phys. Rev. Lett.* **106**, 136802 (2011).
- [14] Q. Liu, C.-X. Liu, C. Xu, X.-L. Qi, and S.-C. Zhang, *Phys. Rev. Lett.* **102**, 156603 (2009).
- [15] See Supplemental Material <http://link.aps.org/supplemental/10.1103/PhysRevLett.110.136601> for experimental and theoretical details.
- [16] Zhe Qu, Leonard Spinu, Huiqiu Yuan, Vladimir Dobrosavljevic, Wei Bao, Jeffrey W. Lynn, M. Nicklas, Jin Peng, Tijiang Liu, David Fobes, Etienne Flesch, and Z. Q. Mao, *Phys. Rev. B* **78**, 180407(R) (2008).
- [17] E. Miranda and V. Dobrosavljevic, *Rep. Prog. Phys.* **68**, 2337 (2005).
- [18] D. Hsieh, Y. Xia, D. Qian, L. Wray, F. Meier, J.H. Dil, J. Osterwalder, L. Patthey, A.V. Fedorov, H. Lin, A. Bansil, D. Grauer, Y.S. Hor, R.J. Cava, and M.Z. Hasan, *Phys. Rev. Lett.* **103**, 146401 (2009).
- [19] R. B. Mallinson, J. A. Rayne, and R. W. Ure, Jr., *Phys. Rev.* **175**, 1049 (1968).
- [20] Y. S. Hor, P. Roushan, H. Beidenkopf, J. Seo, D. Qu, J. G. Checkelsky, L. A. Wray, D. Hsieh, Y. Xia, S.-Y. Xu, D. Qian, M. Z. Hasan, N. P. Ong, A. Yazdani, and R. J. Cava, *Phys. Rev. B* **81**, 195203 (2010).
- [21] T. Dietl, H. Ohno, F. Matsukura, J. Cibert, and D. Ferrand, *Science* **287**, 1019 (2000).